Available online at www.sciencedirect.com
ScienceDirect
Acta Biomaterialia 4 (2008) 1545–1552
Acta BIOMATERIALIA
www.elsevier.com/locate/actabiomat

Nanomechanical properties of surface-modified titanium alloys for biomedical applications

D. Cáceres [a,1], C. Munuera [b], C. Ocal [b], J.A. Jiménez [c], A. Gutiérrez [d], M.F. López [e,*]

[a] Departamento de Física, Escuela Politécnica Superior, Universidad Carlos III, Avda. de la Universidad, 30, 28911 Leganés, Madrid, Spain
[b] Instituto de Ciencia de Materiales de Barcelona, CSIC, Bellaterra, E-08193 Barcelona, Spain
[c] Centro Nacional de Investigaciones Metalúrgicas, CSIC, Avda. Gregorio del Amo 8, E-28040 Madrid, Spain
[d] Departamento de Física Aplicada, Universidad Autónoma de Madrid, Cantoblanco, E-28049 Madrid, Spain
[e] Instituto de Ciencia de Materiales de Madrid, CSIC, Cantoblanco, E-28049 Madrid, Spain

Received 27 November 2007; received in revised form 9 April 2008; accepted 16 April 2008
Available online 30 April 2008

Abstract

The mechanical properties of the oxide layers developed at elevated temperature on three vanadium-free titanium alloys of interest for biomedical applications were investigated by means of the nanoindentation technique. The as-received alloys (Ti–13Nb–13Zr, Ti–15Zr–4Nb and Ti–7Nb–6Al) and their oxide scales formed by reaction with air at 750 °C for several oxidation times were analysed comparatively. In particular, the hardness and the Young's modulus exhibit larger values for the thermally oxidized alloys than for the untreated specimens. However, the Ti–7Nb–6Al alloy shows a different tendency to that of the TiNbZr alloys, which seems to be related to a different oxide layer growth as a function of the oxidation time.

Keywords: Titanium alloys; Nanoindentation; Biomaterials; Oxidation; Hardness

1. Introduction

In the past few years, new Ti alloys have been intensively investigated and developed for biomedical applications as possible substitutes of the well-established Ti–6Al–4V alloy [1–4]. Though this alloy presents excellent mechanical and corrosion properties, it contains vanadium, which is known to be cytotoxic [5,6]. Thus, avoiding metal ion release and obtaining vanadium-free alloys with similar properties has been the focus of interest of recent investigations [7–10]. One important factor, which controls some of the notable properties of pure titanium and its related alloys, is the passive layer, i.e. the native oxide thin film spontaneously formed on the material surface when in contact with air. This protective film is responsible for the excellent corrosion resistance of these materials, which involves low metal ion release even in aggressive environments [11–14]. In order to enhance the corrosion resistance and biocompatibility of Ti alloys, different surface modification techniques have been investigated. Among them, an easy and economic method to generate an oxide film on the surface alloy has been recently proposed. Depending on the alloying elements, this oxide would satisfy the desired surface properties [15,16]. In previous works, some of the properties of three V-free Ti alloys, of composition (in wt.%) Ti–13Nb–13Zr, Ti–15Zr–4Nb and Ti–7Nb–6Al, selected as potential materials for biomedical applications, were investigated before and after oxidation treatments in air at 750 °C [17,18]. The achieved materials were expected to show higher biocompatibility in orthopaedic implants than the most widely used Ti–6Al–4V alloy for two different reasons: the composition of these alloys is free of vanadium, thereby avoiding toxicity problems, and, as expected, the oxidation treatment provides a thicker protective oxide

* Corresponding author. Tel.: +34 913349081; fax: +34 913720623.
E-mail address: mflopez@icmm.csic.es (M.F. López).
[1] Deceased.

1742-7061/$ - see front matter © 2008 Acta Materialia Inc. Published by Elsevier Ltd. All rights reserved.
doi:10.1016/j.actbio.2008.04.009

film than the native oxide. Previous characterization of the surface composition and morphology of these surface-modified alloys has produced very promising results [19–21]. Moreover, highly surface-sensitive scanning force spectroscopy (SFS) measurements have provided some insights into the elasticity properties of their very topmost layer (tens of nanometres) [22]. In Ref. [22], although attempts were made to interpret the elasticity data in terms of alloy composition, their evaluation as a function of indentation depth produced a large dispersion of results. That was an indication of the importance of the specific roughness or composition of the surface. These parameters can differ from those of the bulk material and, consequently, can provide unexpected mechanical properties. Moreover, the gap existing between practical needs and the extremely local information (lateral and vertical) obtained from those scanning force microscopy (SFM) experiments points to the necessity of studying these protective layers on a larger scale (hundreds of nanometres), the region directly in contact with the bone. Important properties that need to be determined include, among others, hardness and Young's modulus. In particular, for a material to be a successful orthopaedic implant it needs a Young's modulus similar to that of bone (10–30 GPa) [23].

Nanoindentation is a non-destructive, versatile and unique technique for determining the mechanical properties of surfaces. When an indentation system is used, loads as small as one nanonewton and displacements of about 0.1 nm can be accurately measured continuously throughout a test. Different mechanical properties can then be determined from the load–displacement data without imaging the indentations [24]. For these reasons, this technique has been used to measure the hardness and Young's modulus of the oxidized films generated as described above. For comparison, this study has also been carried out on untreated alloys.

2. Materials and methods

The three Ti-based alloys were prepared by arc melting and then casting in a copper coquille under high vacuum, using high-purity (better than 99.9%) constituent elements. Therefore, interstitial impurities, such as oxygen, nitrogen, carbon or substitutional transition metals, have just residual values. At this level, the effect of impurities upon the oxidation process of Ti alloys is not significant. The nominal composition of these alloys was (in wt.%) Ti–13Nb–13Zr, Ti–15Zr–4Nb and Ti–7Nb–6Al, which in at.% correspond to $Ti_{84.5}Nb_{7.7}Zr_{7.8}$, $Ti_{89.1}Zr_{8.6}Nb_{2.3}$ and $Ti_{85.9}Al_{10.5}Nb_{3.6}$, respectively. The actual chemical compositions of the alloys in at.% are $Ti_{85.36}Nb_{7.32}Zr_{7.32}$, $Ti_{89.23}Zr_{8.49}Nb_{2.28}$ and $Ti_{84.8}Al_{11.8}Nb_{3.4}$, respectively, as was determined in a previous work [25] by Rutherford backscattering spectroscopy.

The oxidation treatment was performed on samples cut from as-cast ingots by electrospark erosion. Previous to the thermal treatment, the sample surfaces were abraded and polished using diamond paste with successively smaller particle sizes. Colloidal silica was used to ensure a surface free of mechanical deformation. Before performing the oxidation treatment it is important to remove foreign particles and organic contaminant from mechanical polishing. To clean the samples, it is essential to put some gel on the rotating polishing cloth and then to flush with water for approximately 10–15 s before the machine stops. The samples are then cleaned again ultrasonically with acetone and dried with a strong stream of air. After these cleaning steps, optical microscope examination was employed to make sure that there were no residues of silica on the sample surface. Finally, the specimens were cleaned ultrasonically with acetone. The material in this state was named "as-received". The surface cleanness after this procedure was check by X-ray photoemission spectroscopy [26]. At this stage, some samples were isothermally oxidized in air in a tube furnace at 750 °C for exposure times of 1.5 h, 6 h and 24 h.

A microstructural study revealed the existence of two different phases, α and β, whose ratio depended on the alloy composition [17]. The root mean square (rms) roughness values for the three as-received alloys are relatively low (3, 4 and 12 nm for Ti–13Nb–13Zr, Ti–15Zr–4Nb and Ti–7Nb–6Al, respectively) and their surface morphology exhibited two regions with different contrast [21]. This effect might be ascribed to the coexistence of α and β phases since colloidal silica performs selective polishing of each phase due to their different hardnesses.

The cross-sections of the oxidized samples were examined by scanning electron microscopy (SEM) equipped for energy-dispersive X-ray microanalysis. For this analysis, specimens of the three oxidized alloys were submitted to a metallographic preparation, which included mounting the samples in bakelite and polishing by the conventional method. To prevent scale loss during metallographic preparation, the surface of these oxidized samples were coated with a thin gold layer by sputtering. A thicker layer of copper was then deposited electrolytically.

In the present work, nanoindentation tests were made with a Nanoindenter II (Nanoinstruments-MTS Systems, Oak Ridge, TN) using a Berkovich diamond tip. Diamond is the most frequently used indenter material because its high hardness and elastic modulus minimize the contribution of the indenter itself to the measured displacement. For probing properties such as hardness and elastic modulus at the smallest possible scales, the Berkovich triangular pyramidal indenter is preferred over the four-sided Vickers or Knoop indenter because a three-sided pyramid is more easily ground to a sharp point.

Each specimen was tested at room temperature using the continuous stiffness measurement (CSM) technique developed by Oliver and Pethica [27,28]. The CSM is accomplished by imposing a small, sinusoidally varying signal on top of a DC signal that drives the motion of the indenter. The data are obtained by analysing the response of the system by means of a frequency-specific amplifier. This

allows the measurement of contact stiffness at any point along the loading curve and not just at the point of unloading as in the conventional measurement. The CSM technique makes possible the continuous measurement of mechanical properties in one experiment without the need of discrete unloading cycles. Moreover, the time constant is at least three orders of magnitude smaller than that of the more conventional method. The measurements can be made at extremely small penetration depths. The contact stiffness, applied load and indenter displacement can then be used to determine the mechanical properties as a function of the indenter depth. This technique is thus ideal for non-uniform materials, such as oxidized layer in Ti alloys, since the microstructure and mechanical properties change with indentation depth. In the present work, a minimum of 10 indentations were made in each specimen. Afterwards, the statistical mean value with its corresponding standard deviation was calculated for 25 nm width windows of the tip contact displacement values. Eventually, the mean values were taken as the final hardness (H) and Young's modulus (E) values.

3. Results and discussion

The hardness (H) and elastic Young's modulus (E) of the as-received Ti–13Nb–13Zr, Ti–15Zr–4Nb and Ti–7Nb–6Al surfaces obtained by using the nanoindentation technique are depicted in Fig. 1 as a function of indentation depth. For indentations smaller than 100 nm, E can be as low as 50 GPa, in agreement with the very surface sensitive data obtained in a previous SFS study for the same samples [22]. After this regime, the values of both magnitudes are higher for the aluminium-containing alloy than for the two TiNbZr alloys. The lowest value corresponded to Ti–13Nb–13Zr. Note that although hardness values, in particular, have large error bars, the Young's modulus values are within the range of bulk properties for pure Ti and Ti–6Al–4V alloys, which are around 100–120 GPa [29]. Since all three materials are α–β Ti alloys and nanoindentations were performed at randomly chosen locations, the non-negligible scatter between individual measurements should be related to the combination of at least two different factors: (i) a different hardness value of the α and β phases, whose contribution would depend on the corresponding β-phase/α-phase ratio existing within the tested area in each alloy; and (ii) a significant influence of the crystal orientation on the nanoscale mechanical properties [30]. To minimize these position-dependent factors, the data presented are, as mentioned above, the statistical mean values calculated from at least 10 measurements.

An inspection of Fig. 1 shows an increase in the measurement error bars as we approach the surface. Since these differences were observed in the three alloys used in this study, they were associated with the experimental conditions. This could be a combination of errors in depth determination at the very small contact displacement and the greater effect of the surface roughness, which can set a lower limit to the useful nanoindentation size.

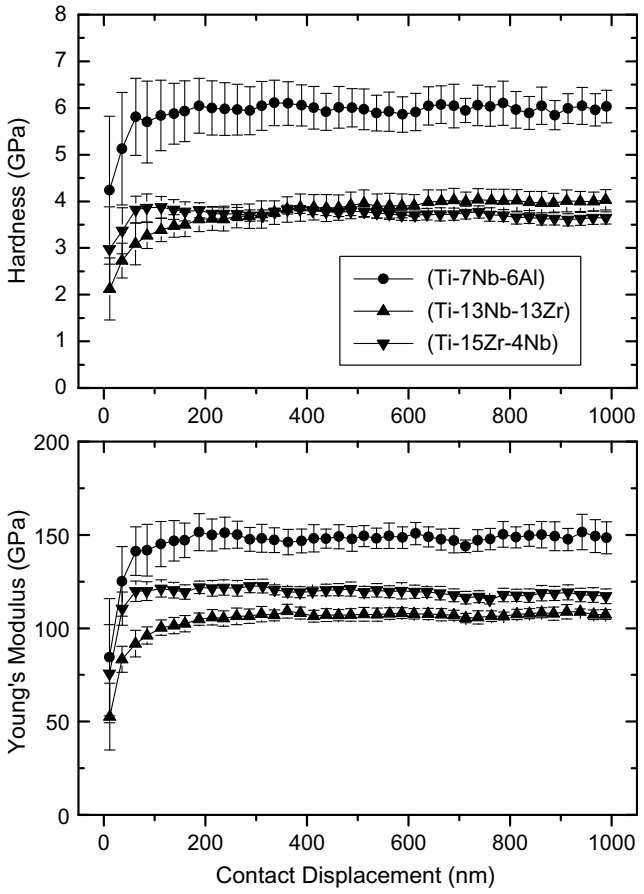

Fig. 1. Hardness and Young's modulus for the Ti–13Nb–13Zr, Ti–15Zr–4Nb and Ti–7Nb–6Al alloys in the as-received condition.

Taking into account that the body-centred cubic β-Ti exhibits lower Young's modulus values (60–80 GPa) than the hexagonal close-packed α-Ti (100–120 GPa) [29], the alloy with the highest β-phase/α-phase ratio is expected to have the lowest Young's modulus. This prediction is corroborated empirically by the data depicted in the figure. From a previous SEM study [17], the β-phase/α-phase ratio is known to be different for each of the three Ti-based alloys. In particular, Ti–13Nb–13Zr has the highest β-phase/α-phase ratio and the lowest elastic modulus measured here. However, whereas Ti–7Nb–6Al and Ti–15Zr–4Nb alloys show similar β-phase/α-phase ratios, they exhibit different nanomechanical values, as inferred from Fig. 1. This discrepancy can be explained in terms of the difference in some of the alloying elements of these materials and the consequent effect on their solid solution strengthening.

Being aware of the importance of structural features for small-scale investigations of mechanical properties, the cross-sectional views of the three alloys after oxidation at 750 °C for 24 h are depicted in the SEM micrographs of Fig. 2. The thickness of the oxide layer is about 10 μm for Ti–13Nb–13Zr, 25 μm for Ti–15Zr–4Nb and 2 μm for

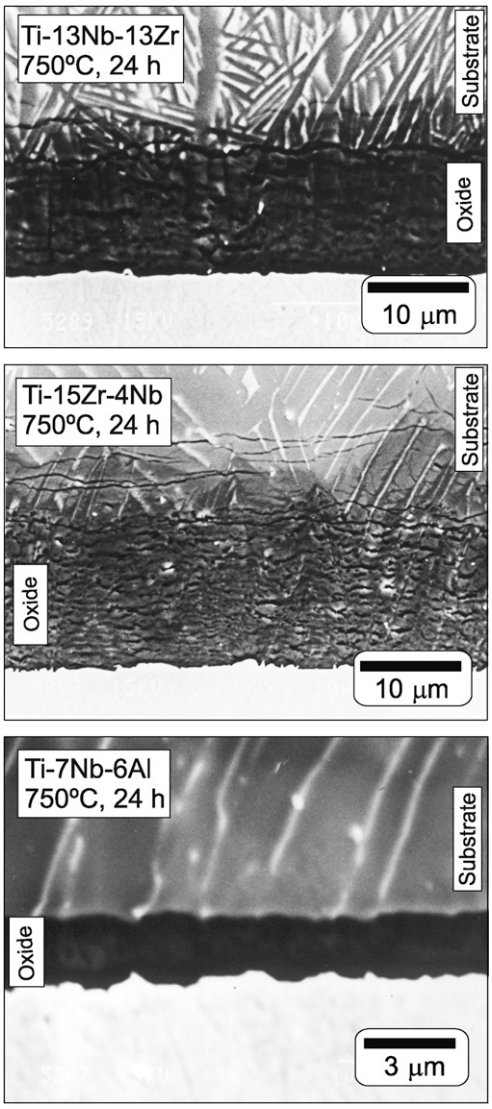

Fig. 2. Cross-sectional SEM micrographs of Ti–13Nb–13Zr, Ti–15Zr–4Nb and Ti–7Nb–6Al after oxidation treatment at 750 °C for 24 h.

Ti–7Nb–6Al. As can be observed, the presence of numerous pores within the scales and some longitudinal fissures at the metal–oxide interface is evident in the case of the two TiNbZr alloys. As discussed below, the lack of structural quality of the oxide layers is at the origin of the broader range of nanoindentation data for the oxidized alloys as compared to their as-received counterpart. In particular, the fissures and porosity would lead to a given degree of uncertainty related to the specific testing position for each measurement. This is evidenced in the SFM image of Fig. 3, which shows for one of the samples how these structural defects reach the oxide layer surface, causing the formation of ridges and grooves (up to 500 nm deep). The subsequent surface roughness also plays an important role in the response of the material in the nanoindentation process. Previous SFM investigations showed a much higher rms surface roughness for the scale as compared to the values measured in the as-received samples [21]. In

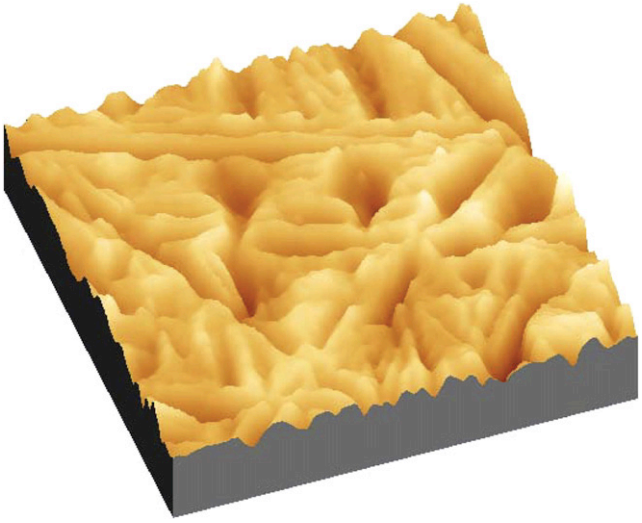

Fig. 3. SFM topographic image (10 μm lateral size) of Ti–15Zr–4Nb after oxidation treatment at 750 °C for 24 h. The total z-scale is 1.8 μm.

the case of the TiNbZr alloys, the rms surface roughness was found to be approximately constant after 1.5 h of treatment at 750 °C and within the range of the oxidation time analysed. The values were approximately 150 nm for Ti–13Nb–13Zr alloy and 275 nm for Ti–15Zr–4Nb.

Though the biological properties of the oxidized alloys have not been evaluated in the present work, improvement in the biocompatibility and osseointegration capability, associated to the changes in chemical composition and roughness of the surface, is expected. The existence of titanium oxide on the Ti surface has been reported to improve bone formation [31–33]. On the other hand, relatively rougher surfaces exhibit higher contents and better distribution of protein deposits onto Ti surfaces, which positively affects the cellular response to osseous healing [34]. Furthermore, investigations on cellular adhesion to bones as a function of surface roughness have produced superior results with rough surfaces, confirming the beneficial effect of surface oxidation on the deposition of osteoblastic cells and corresponding improvement in osseointegration [35].

Figs. 4 and 5 show the hardness and Young's modulus values vs. the indentation depth for the oxidized Ti–13Nb–13Zr and Ti–15Zr–4Nb, respectively. The data for the as-received alloys are included for comparison. Both, hardness and Young's modulus are somewhat independent of oxidation time, but appear to be higher than those of the corresponding as-received alloys. This effect is due to the presence of the protective oxide layer generated during the heat treatment. As has previously been shown for both TiNbZr alloys, the oxide layer generated on the material surface during oxidation in air at 750 °C for time periods of 1.5, 6 and 24 h is composed mainly of TiO_2 [19]. However, the average hardness and Young's modulus values obtained in the present study are lower than those reported in the literature for rutile [36,37]. This result seems to be related to the porosity and fissures of the TiO_2 oxide layer

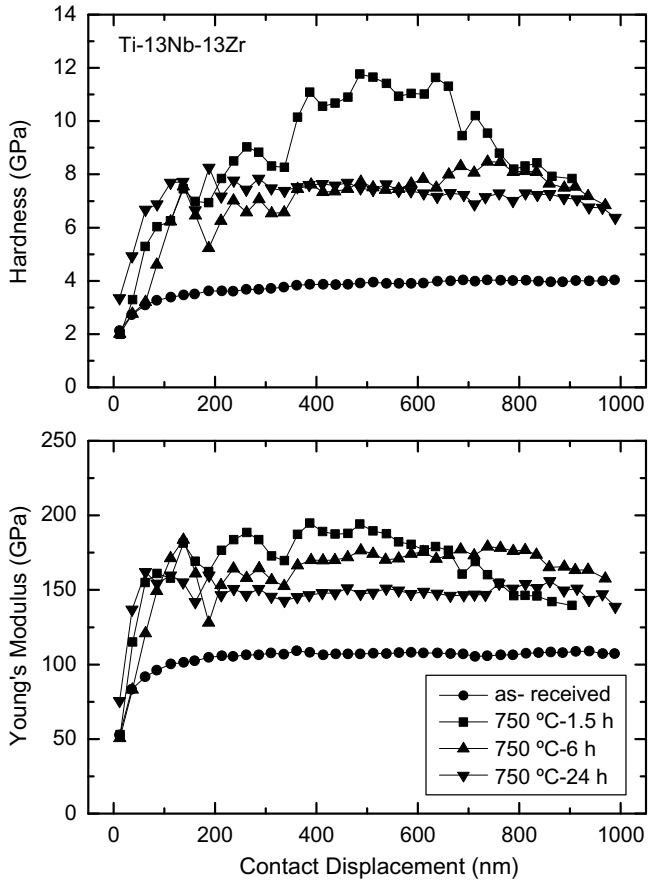

Fig. 4. Hardness and Young's modulus for the as-received and heat-treated Ti–13Nb–13Zr alloys.

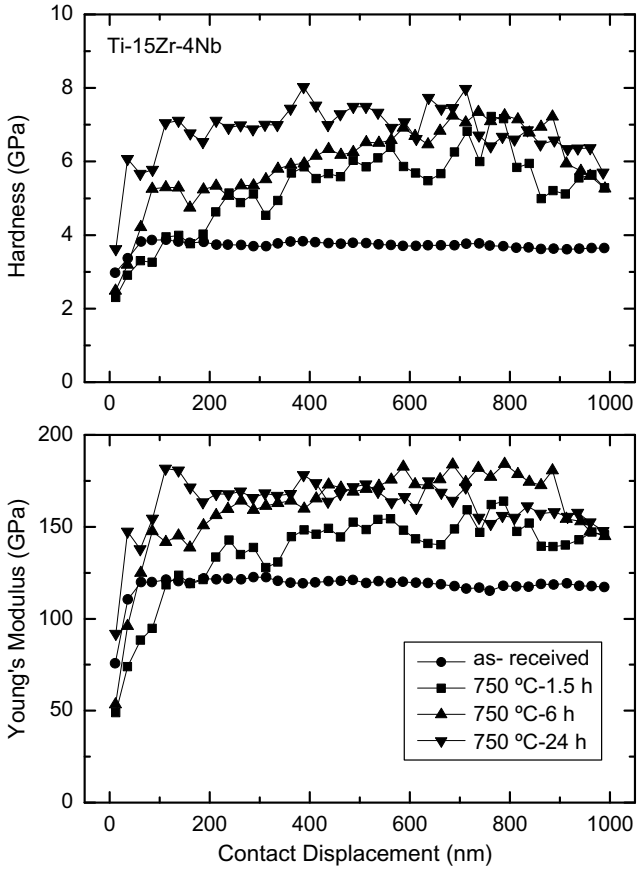

Fig. 5. Hardness and Young's modulus for the as-received and heat-treated Ti–15Zr–4Nb alloys.

formed on the two TiNbZr alloys, which is not observed for TiO_2 rutile samples.

The hardness and Young's modulus for the Ti–7Nb–6Al alloy and the oxide layers generated during the same three treatment times are depicted in Fig. 6. Both magnitudes follow a similar tendency, presenting a transient region, which is wider for large oxidation times, of continuous increase until saturation is reached. The final value at the deeper indentation displacement, even in the case of the heaviest oxidation after 24 h, is close to that for the as-received sample. This result is in contrast to what happened for the TiNbZr alloys, where hardness and Young's modulus values at the maximum contact displacement were always higher for the oxidized samples. This effect can be attributed to the presence of a thicker oxide layer in the oxidized TiNbZr alloys, which leads to a lower substrate effect than in the case of the oxidized TiNbAl samples.

The continuous increase of the displacement threshold, at which maximum values of hardness and elastic modulus are reached, for the Ti–7Nb–6Al is correlated to the continuous linear increase of the rms for this alloy [21]. However, this result cannot be related to the development of pores on the scale because the oxide layer developed is quite compact, as shown in Fig. 2. Therefore, the effect observed in Fig. 6 seems to be related to the outer layer composition of the oxidized Ti–7Nb–6Al, which has been shown to evolve with oxidation time [19]. In the early stages of thermal treatment, an outer layer of Al_2TiO_5 is formed. On top of this an Al_2O_3-rich film is developed, which becomes thicker with oxidation time.

The evolution of the hardness and Young's modulus with oxidation time apparently contradicts the formation of a continuous Al_2O_3 layer, which would be expected to promote an enhancement of the nanomechanical values on the surface region when the Ti–7Nb–6Al alloy is progressively oxidized. However, previous SFM studies on this oxidized sample have shown that a columnar growth takes place [38]. Thus, the formation of columnar Al_2O_3 grains could be responsible for the low values for hardness and Young's modulus, since this type of structure favours easier penetration into the surface. Consequently, both H and E increase gradually with distance from the surface, until the inner Al_2TiO_5 layer is reached. For deeper contact displacements a tendency towards the as-received alloy properties is observed. The fact that the Al_2O_3 layer increases with oxidation time also explains the differences in the nanoindentation results obtained in these samples with those obtained for the aluminium free ones, where the plateau was reached at lower contact displacement values. The contact depth at which the plateau region is reached clearly increases with oxidation time, as can be observed in

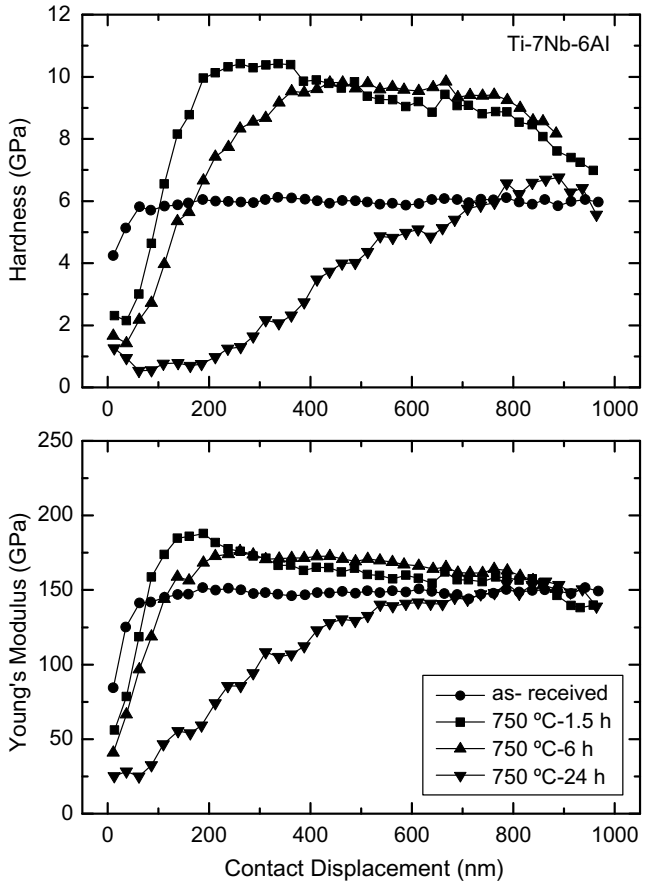

Fig. 6. Hardness and Young's modulus for the as-received and heat-treated Ti–7Nb–6Al alloys.

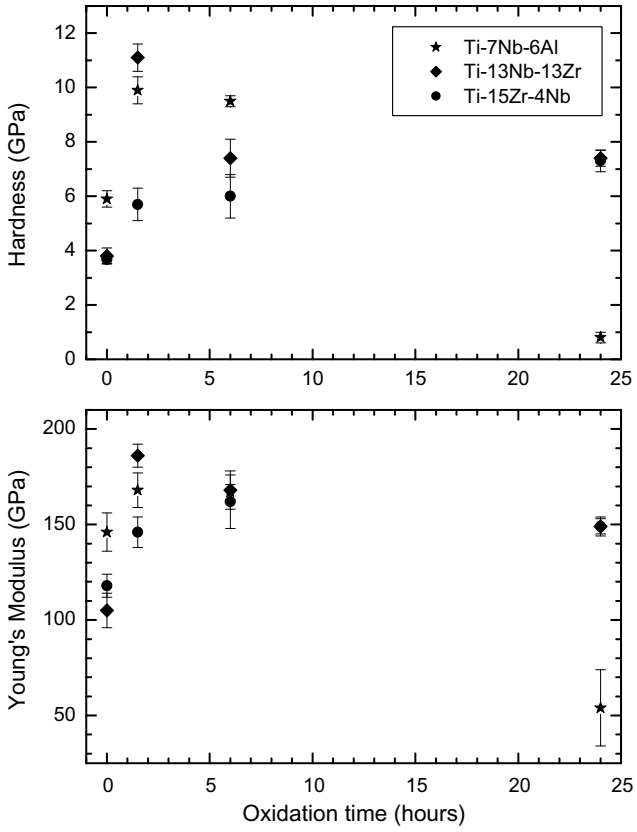

Fig. 7. Evolution of the hardness and Young's modulus for the different surface scales as a function of oxidation time.

Fig. 6. At the first stages of the thermal process (1.5 h of oxidation time) the columnar structure is located close to the surface and affects the nanoindentation results up to about 200 nm. As the oxidation time is increased to 6 h, the Al_2O_3 columnar structure region becomes wider and, consequently, affects deeper nanoindentation data, up to about 400 nm. Finally, for the case of the 24 h oxidized Ti–7Nb–6Al alloy, with the deepest columnar Al_2O_3 structure, all the range measured by nanoindentation seems to be affected by this columnar structure and almost no plateau is reached.

In order to show the effect of the oxidation time on the properties of the scales generated on the different alloys, Fig. 7 summarises the results for all layers. The depicted hardness and Young's modulus values for the Ti–13Nb–13Zr and Ti–15Zr–4Nb alloys correspond to the statistical mean values and their corresponding standard deviations, calculated taking all the values in the plateau zone of the different graphs representing H and E vs. contact displacement of the indenter (Figs. 4 and 5). We chose the values in the plateau because they are considered to be unaffected by any influence of the substrate [39,40]. In the case of Ti–7Nb–6Al, the region corresponding to the columnar Al_2O_3 structure was avoided. The values for the sample with an oxidation time of 1.5 h were calculated by considering the mean value in the plateau from 200 to 750 nm, while for the 6 h oxidation time sample the plateau region was considered from 400 to 750 nm. After 24 h of oxidation, since almost all the measured range was affected by the columnar Al_2O_3 structure, it was not possible to determine either the hardness or the Young's modulus value for this sample.

In the case of Ti–13Nb–13Zr, the most relevant feature is the considerable increase of 7 GPa in H and of 80 GPa in E at an oxidation time of only 1.5 h, followed by a decrease in these values as the oxidation time increases. The Ti–15Zr–4Nb alloy presents a smoother, continuous increase in the hardness values as a function of oxidation time, reaching a maximum increase of H of about 3 GPa after 24 h and a total increase of E of 45 GPa. The different percentages of alloying elements in each material seems to determine the different ways in which the nanomechanical properties evolve. A threefold different Zr/Nb ratio in the bulk chemical composition would certainly promote different diffusion processes at the temperatures studied. And, even though the main component is TiO_2 for both oxidized alloys, different percentages of Ti, Nb and Zr oxides are obtained on the surfaces of Ti–13Nb–13Zr and Ti–15Zr–4Nb [20,26]. Independently of the way that oxidation progresses, after 24 h of heat treatment, both TiNbZr alloys present almost the same hardness and Young's modulus values.

The aluminium-containing alloy has a different tendency. There is a noticeable decrease in both H and E for long oxidation times in the case of Ti–7Nb–6Al. Initially, an increase in hardness of 4 GPa and an increase in Young's modulus of 20 GPa are observed. These remain almost constant for 6 h of oxidation, but then the structural changes noted take place for longer oxidation times, leading to the important decreases in mechanical properties.

4. Conclusions

The systematic analysis of the mechanical properties, in particular hardness and Young's modulus, obtained by the nanoindentation technique of three different vanadium-free Ti alloys and their oxide layers, of interest as biomaterials, has been presented. The results have been interpreted in combination with previous results on the same materials in order to bridge the gap between extremely surface-sensitive techniques, which led to relatively high uncertainty and a wide spread data, and practical needs. This has enabled us to make the following conclusions:

1. Hardness and Young's modulus mean values measured for the Ti–13Nb–13Zr, Ti–15Zr–4Nb and Ti–7Nb–6Al alloys in the as-received condition fall within the range of bulk properties for pure Ti and Ti–6Al–4V alloys. However, the different compositions and β-phase/α-phase ratios of the alloys yield a number of differences. The highest β-phase/α-phase ratio of the Ti–13Nb–13Zr alloy provides the lowest hardness and Young's modulus values. On the other hand, the presence of Al instead of Zr in the Ti–7Nb–6Al alloy seems to be at the origin of its highest surface mechanical properties values.
2. During oxidation at 750 °C, an oxide layer, composed mainly of TiO_2, is generated on the surface of the TiNbZr alloys. Hardness and Young's modulus mean values measured for both oxidized TiNbZr alloys are higher than those corresponding to the as-received specimens. However, the surface roughness and the presence of many pores on the scales cause lower hardness and Young's modulus than those reported in the literature for rutile.
3. The formation of columnar structures during the oxide layer growing on the Ti–7Nb–6Al alloy plays a significant role in its surface mechanical behaviour and leads to a fall in both hardness and Young's modulus for long oxidation times. This reaches a value close to that suitable for implant materials at the longer oxidation treatment studied here.

Acknowledgements

We gratefully acknowledge Prof. G. Fommeyer from Max Planck Institut für Eisenforschung (Düsseldorf) for kindly supplying the Ti alloys specimens. This work was partially supported by the Spanish "Programa de Tecnología de los Materiales de la Comunidad Autónoma de Madrid" under Projects 07N-0050-1999 and 07N-0066-2002, and by the Spanish MEC under Projects MAT-2006-13348, MAT2007-66719-C03-03, MAT2007-62732 and "Nanoselect" of the Spanish Consolider-Ingenio 2007 program.

References

[1] Trentani L, Pelillo F, Pavesi FC, Ceciliani L, Cetta G, Forlino A. Evaluation of the TiMo12Zr6Fe2 alloy for orthopaedic implants: in vitro biocompatibility study by using primary human fibroblasts and osteoblasts. Biomaterials 2002;23:2863–9.
[2] Maehara K, Doi K, Matsushita T, Sasaki Y. Application of vanadium-free titanium alloys to artificial hip joints. Mater Trans 2002;43:2936–42.
[3] Lin DJ, Chern Lin JH, Ju CP. Structure and properties of Ti–7.5Mo–xFe alloys. Biomaterials 2002;23:1723–30.
[4] Kobayashi S, Nakagawa S, Nakai K, Ohmori Y. Phase decomposition in a Ti–13Nb–13Zr alloy during aging at 600 degrees C. Mater Trans 2002;43:2956–63.
[5] Steinemann SG. Corrosion of surgical implants – in vivo and in vitro tests. In: Winter GD, Leray JL, de Groot K, editors. Evaluation of biomaterials. New York: Wiley; 1980. p. 1–34.
[6] Okazaki Y, Nishimura E. Effect of metal released from Ti alloy wear powder on cell viability. Mater Trans JIM 2000;41:1247–55.
[7] Okazaki Y, Rao S, Ito Y, Tateishi T. Corrosion resistance, mechanical properties, corrosion fatigue strength and cytocompatibility of new Ti alloys without Al and V. Biomaterials 1998;19:1197–215.
[8] Ho WF, Ju CP, Chern Lin JH. Structure and properties of cast binary Ti–Mo alloys. Biomaterials 1999;20:2115–22.
[9] Oliveira NTC, Ferreira EA, Duarte LT, Biaggio SR, Rocha-Filho RC, Bocchi N. Corrosion resistance of anodic oxides on the Ti–50Zr and Ti–13Nb–13Zr alloys. Electrochim Acta 2006;51:2068–75.
[10] Hao YL, Li SJ, Sun SY, Zheng CY, Yang R. Elastic deformation behaviour of Ti–24Nb–4Zr–7.9Sn for biomedical applications. Acta Biomater 2007;3:277–86.
[11] Dugdale I, Cotton JB. The anodic polarization of titanium in halide solutions. Corros Sci 1964;4:397–411.
[12] Pan J, Thierry D, Leygraf C. Electrochemical impedance spectroscopy study of the passive oxide film on titanium for implant application. Electrochim Acta 1996;41:1143–53.
[13] Gonzalez JEG, Mirza-Rosca JC. Study of the corrosion behavior of titanium and some of its alloys for biomedical and dental implant applications. J Electroanal Chem 1999;471:109–15.
[14] Tamilselvi S, Raman V, Rajendran N. Corrosion behaviour of Ti–6Al–7Nb and Ti–6Al–4V ELI alloys in the simulated body fluid solution by electrochemical impedance spectroscopy. Electrochim Acta 2006;52:839–46.
[15] López MF, Gutiérrez A, García-Alonso MC, Escudero ML. Surface analysis of a heat-treated, Al-containing, iron-based superalloy. J Mater Res 1998;13:3411–6.
[16] Escudero ML, López MF, Ruiz J, García-Alonso MC, Canahua H. Comparative study of the corrosion behaviour of MA-956 and conventional metallic biomaterials. J Biomed Mater Res 1996;31:313–7.
[17] López MF, Gutiérrez A, Jiménez JA. In vitro corrosion behaviour of titanium alloys without vanadium. Electrochim Acta 2002;47:1359–64.
[18] López MF, Jiménez JA, Gutiérrez A. Corrosion study of surface-modified vanadium-free titanium alloys. Electrochim Acta 2003;48:1395–401.
[19] López MF, Soriano L, Palomares FJ, Sánchez-Agudo M, Fuentes GG, Gutiérrez A, et al. Soft X-ray absorption spectroscopy study of oxide layers on titanium alloys. Surf Interface Anal 2002;33:570–6.
[20] Gutiérrez A, López MF, Jiménez JA, Morant C, Paszti F, Climent A. Surface characterization of the oxide layer grown on Ti–Nb–Zr and Ti–Nb–Al alloys. Surf Interface Anal 2004;36:977–80.

[21] Gutiérrez A, Munuera C, López MF, Jiménez JA, Morant C, Matzelle T, et al. Surface microstructure of the oxide protective layers grown on vanadium-free Ti alloys for use in biomedical applications. Surf Sci 2006;600:3780–4.
[22] Munuera C, Matzelle TR, Kruse N, López MF, Gutiérrez A, Jiménez JA, et al. Surface elastic properties of Ti alloys modified for medical implants: a force spectroscopy study. Acta Biomater 2007;3:113–9.
[23] Reilly DT, Burstein AH. The elastic and ultimate properties of compact bone tissue. J Biomech 1975;8:393–405.
[24] Bhushan B. Handbook of micro/nanotribology. 2nd ed. Boca Raton, FL: CRC Press; 1999.
[25] Gutiérrez A, Pászti F, Climent-Font A, Jiménez JA, López MF. A comparative study of the oxide scale thermally grown on titanium alloys by ion beam analysis techniques and scanning electron microscopy. J Mater Res, in press.
[26] López MF, Gutiérrez A, Jiménez JA. Surface characterization of new non-toxic titanium alloys for use as biomaterials. Surf Sci 2001;482:300–5.
[27] Pethica JB, Oliver WC. Mechanical properties of nanometer volumes of material: use of the elastic response of small area indentation. Mater Res Soc Symp Proc 1989;130:13–23.
[28] Oliver WC, Pharr GM. An improved technique for determining hardness and elastic-modulus using load and displacement sensing indentation experiments. J Mater Res 1992;7:1564–83.
[29] Niinomi M. Recent metallic materials for biomedical applications. Metall Mater Trans A 2002;33:477–86.
[30] Viswanathan GB, Lee E, Maher DM, Banerjee S, Fraser HL. Direct observations and analyses of dislocation substructures in the α phase of an α/β Ti-alloy formed by nanoindentation. Acta Mater 2005;53:5101–15.
[31] Sul YT, Johansson CB, Jeong Y, Röser K, Wennerberg A, Albrektsson T. Oxidized implants and their influence on the bone response. J Mater Sci Mater Med 2001;12:1025–31.
[32] Sul YT. The significance of the surface properties of oxidized titanium to the bone response: special emphasis on potential biochemical bonding of oxidized titanium implant. Biomaterials 2003;24:3893–907.
[33] Thomsen P, Larsson C, Ericson LE, Sennerby L, Lausmaa J, Kasemo B. Structure of the interface between rabbit cortical bone and implants of gold, zirconium and titanium. J Mater Sci Mater Med 1997;8:653–65.
[34] Stanford CM, Keller JC, Solursh M. Bone cell expression on titanium surfaces is altered by sterilization treatments. J Dent Res 1994;73:1061–71.
[35] Larsson C, Thomsen P, Aronsson BO, Rodahl M, Lausmaa J, Kasemo B, et al. Bone response to surface-modified titanium implants: studies on the early tissue response to machined and electropolished implants with different oxide thicknesses. Biomaterials 1996;17:605–16.
[36] Stollberg DW, Hampikian JM, Riester L, Carter WB. Nanoindentation measurements of combustion CVD Al2O3 and YSZ films. Mater Sci Eng A 2003;359:112–8.
[37] Gong JH, Peng ZJ, Miao HZ. Analysis of the nanoindentation load–displacement curves measured on high-purity fine-grained alumina. J Eur Ceram Soc 2005;25:649–54.
[38] Morant C, López MF, Gutiérrez A, Jiménez JA. AFM and SEM characterization of non-toxic vanadium-free Ti alloys used as biomaterials. Appl Surf Sci 2003;220:79–87.
[39] Oliver WC, Hutchings R, Pethica JB. Measurement of hardness at indentation depths as low as 20 nanometers. In: Blau PJ, Lawn BR, editors. Microindentation techniques in materials science and engineering. ASTM STP. West Conshohocken, PA: American Society for Testing and Materials; 1986. p. 90–108.
[40] Tayebi N, Pojycarpou AA, Conry TF. Effects of substrate on determination of hardness of thin films by nanoscratch and nanoindentation techniques. J Mat Res 2004;19:1791–802.